1521-0103/344/2/511–521$25.00
THE JOURNAL OF PHARMACOLOGY AND EXPERIMENTAL THERAPEUTICS

http://dx.doi.org/10.1124/jpet.112.199745
J Pharmacol Exp Ther 344:511–521, February 2013

Expression and Activity of Nitric Oxide Synthase Isoforms in Methamphetamine-Induced Striatal Dopamine Toxicity

Danielle M. Friend, Jong H. Son, Kristen A. Keefe, and Ashley N. Fricks-Gleason

Interdepartmental Program in Neuroscience (D.M.F., K.A.K.) and Department of Pharmacology and Toxicology (J.H.S., K.A.K., A.N.F.), University of Utah, Salt Lake City, Utah

Received September 7, 2012; accepted December 7, 2012

ABSTRACT

Nitric oxide is implicated in methamphetamine (METH)-induced neurotoxicity; however, the source of the nitric oxide has not been identified. Previous work has also revealed that animals with partial dopamine loss induced by a neurotoxic regimen of methamphetamine fail to exhibit further decreases in striatal dopamine when re-exposed to methamphetamine 7–30 days later. The current study examined nitric oxide synthase expression and activity and protein nitration in striata of animals administered saline or neurotoxic regimens of methamphetamine at postnatal days 60 and/or 90, resulting in four treatment groups: Saline:Saline, METH:Saline, Saline:METH, and METH:METH. Acute administration of methamphetamine on postnatal day 90 (Saline:METH and METH:METH) increased nitric oxide production, as evidenced by increased protein nitration. Methamphetamine did not, however, change the expression of endothelial or inducible isoforms of nitric oxide synthase, nor did it change the number of cells positive for neuronal nitric oxide synthase mRNA expression or the amount of neuronal nitric oxide synthase mRNA per cell. However, nitric oxide synthase activity in striatal interneurons was increased in the Saline:METH and METH:METH animals. These data suggest that increased nitric oxide production after a neurotoxic regimen of methamphetamine results from increased nitric oxide synthase activity, rather than an induction of mRNA, and that constitutively expressed neuronal nitric oxide synthase is the most likely source of nitric oxide after methamphetamine administration. Of interest, animals rendered resistant to further methamphetamine-induced dopamine depletions still show equivalent degrees of methamphetamine-induced nitric oxide production, suggesting that nitric oxide production alone in response to methamphetamine is not sufficient to induce acute neurotoxic injury.

Introduction

It is estimated that 60 million people worldwide have abused amphetamine-type psychostimulants, including methamphetamine (METH; Maxwell, 2005). METH abuse results in selective damage to central monoamine systems. In particular, repeated high-dose administration of METH results in persistent dopamine (DA) deficits in rodents, nonhuman primates, and humans. These DA deficits are manifested as decreases in DA concentration (Kogan et al., 1976; Wagner et al., 1980), DA transporter (DAT; Volkow et al., 2001; Guilarte et al., 2003) and vesicular monoamine transporter-2 levels (Guilarte et al., 2003), and tyrosine hydroxylase activity (Kogan et al., 1976), particularly in striatum. The exact mechanisms contributing to this phenomenon have yet to be fully elucidated; however, a number of factors occurring during or shortly after administration of a neurotoxic regimen of METH, including the production of nitric oxide (NO), have been implicated in this toxicity.

NO production is involved in a variety of normal physiologic process and various pathologic conditions. NO is produced by nitric oxide synthase (NOS), of which there are three isoforms: neuronal nitric oxide synthase (nNOS), inducible nitric oxide synthase (iNOS), and endothelial nitric oxide synthase (eNOS). The work of several groups has suggested an important role for NO in METH-induced monoamine system damage. First, NO can interact with oxygen to form peroxynitrite, a potent oxidant (Radi et al., 1991). Second, prior studies have suggested that nNOS protein (Deng and Cadet, 1999), nitrate (Anderson and Itzhak, 2006), and protein nitration—an indirect measure of peroxynitrite

This work was supported by the National Institutes of Health National Institute on Drug Abuse [Grants DA 013367 and DA 031523].

Portions of this work were previously presented at the following meetings: Friend DM, Keefe KA, Chen P (2009) nNOS & iNOS expression in resistance to methamphetamine neurotoxicity. *The Society for Neuroscience*; 2009 Oct 17-21; Chicago, IL. Friend DM, Fricks-Gleason AN, Chen P, Keefe KA (2010) Expression of NOS isoforms in methamphetamine-induced striatal dopamine toxicity. *International Basal Ganglia Society*; 2010 June 20-24; Long Branch, NJ. Friend DM, Fricks-Gleason AN, Chen P, Hanson GR, Keefe KA (2010) Expression of NOS isoforms in methamphetamine-induced striatal dopamine toxicity. *Translational Research in Methamphetamine Addiction*; 2010 Jul 19-21; Pray, MT. Friend DM, Fricks-Gleason AN, Keefe KA (2010) Expression of NOS isoforms in methamphetamine-induced striatal dopamine neurotoxicity. *The Society for Neuroscience*; 2010 Nov 13-17; San Diego, CA. Friend DM, Fricks-Gleason AN, Keefe, KA (2010) NOS isoform expression and activity in methamphetamine-induced striatal dopamine toxicity. *Gordon Research Conference on Catecholamines*; 2010 Aug 6-12; Lewiston, ME. Friend DM, Fricks-Gleason AN, Keefe, KA (2011) Nitric oxide synthase isoform expression and activity in methamphetamine-induced striatal neurotoxicity. *Winter Conference on Brain Research*; 2011 Jan 21-26; Snowbird, UT.

dx.doi.org/10.1124/jpet.112.199745.

ABBREVIATIONS: ANOVA, analysis of variance; DA, dopamine; DAT, dopamine transporter; eNOS, endothelial nitric oxide synthase; GLU, glutamate; iNOS, inducible nitric oxide synthase; MANOVA, multivariate ANOVA; METH, methamphetamine; NMDA, *N*-methyl-D-aspartate; NO, nitric oxide; NOS, nitric oxide synthase; nNOS, neuronal nitric oxide synthase; PBS, phosphate-buffered saline; PND, postnatal day.

production (Imam et al., 1999; Imam et al., 2000)—are increased in striatum after METH exposure. Third, coadministration of peroxynitrite decomposition catalysts prevents METH-induced DA depletions (Imam et al., 1999). Fourth, METH-induced DA depletions are blocked in mice with deletion of nNOS (Itzhak et al., 1998; Itzhak et al., 2000b) and partially attenuated in mice with deletion of iNOS (Itzhak et al., 1999; Itzhak et al., 2000b). However, the use of peroxynitrite decomposition catalysts and nNOS and iNOS knockout mice also mitigated METH-induced hyperthermia (Itzhak et al., 1998; Imam et al., 1999; Itzhak et al., 1999) known to be critical for METH-induced monoamine toxicity (Ali et al., 1994). In addition, studies using pharmacological inhibitors of NOS are similarly inconclusive. Some studies suggest protection against METH-induced DA depletions when NOS inhibitors are coadministered (Di Monte et al., 1996; Itzhak and Ali, 1996; Ali and Itzhak, 1998; Itzhak et al., 2000a), whereas others suggest that the neuroprotective effects of NOS inhibitors result from mitigation of METH-induced hyperthermia (Taraska and Finnegan, 1997; Callahan and Ricaurte, 1998). Adding to the debate on the role of NO production in METH-induced neurotoxicity are data demonstrating that the elimination of nNOS-expressing cells in striatum fails to protect against METH-induced tyrosine hydroxylase depletions (Zhu et al., 2006).

To further explore factors sufficient for METH-induced monoamine toxicity, we have used a model of resistance to this toxicity, in which animals are treated with a binge regimen of METH but do not show acute monoamine toxicity. That is, our laboratory and others have conducted studies in which animals are treated with a neurotoxic regimen of METH and are challenged seven or 30 days later with a second neurotoxic regimen of METH. The data from these studies show that animals with partial DA loss induced by an initial exposure to a neurotoxic regimen of METH fail to exhibit further DA, DAT, and vesicular monoamine transporter-2 depletions when exposed to the second neurotoxic regimen (Thomas and Kuhn, 2005; Hanson et al., 2009). The extent to which this resistance to subsequent METH-induced neurotoxicity is associated with decreased NO production is unknown. Thus, the purpose of the current study was to determine the source of NO after METH exposure and to examine whether animals rendered resistant to further METH-induced DA depletions have decreases in NO production.

Materials and Methods

Animals. Male Sprague-Dawley rats (Charles River Laboratories, Raleigh, NC) were housed in wire mesh cages in a temperature-controlled room on a 12:12-hour light/dark cycle with free access to food and water. All animal care and experimental procedures were in accordance with the *Guide for the Care and Use of Laboratory Animals* (8^{th} Ed., National Research Council) and were approved by the Institutional Animal Care and Use Committee at the University of Utah.

METH Administration. On days of METH injections (postnatal days [PNDs] 60 and 90), rats were housed in groups of four in plastic tub cages (33 cm × 28 cm × 17 cm) with corncob bedding. Rats were given injections of (±)-METH•HCl (National Institutes of Health National Institute on Drug Abuse, Bethesda, MD; 10 mg/kg, free base, subcutaneous) or 0.9% saline (1 ml/kg, subcutaneous) at 2-hour intervals for a total of four injections. This METH dosing regimen has previously been shown to significantly reduce DA levels and tyrosine hydroxylase activity in the striatum (Kogan et al., 1976). To monitor METH-induced hyperthermia, rectal temperatures were recorded using a digital thermometer (BAT-12; Physitemp Instruments, Clifton, NJ). Temperatures were taken 30 minutes before the first injection of saline or METH and 1 hour after each injection thereafter. Animals whose core temperature exceeded 40.5°C were cooled by placement in a cool chamber until their core temperature decreased below 39°C. Eighteen hours after the last injection of METH or saline on PND60, animals were returned to their home cages and allowed to recover for 30 days. On PND90, animals were again housed in plastic tub cages as described above and injected with either saline or the neurotoxic regimen of METH, similar to PND60 treatments. This experimental protocol resulted in four treatment groups based on treatments on PND60 and PND90 (PND60:PND90): Saline:Saline, Saline:METH, METH:Saline, and METH:METH. Animals were sacrificed 1 hour or 48 hours after their last injection on PND90.

Tissue Preparation. Rats were sacrificed by exposure to carbon dioxide for 1 minute, followed by decapitation. To perform both in situ hybridization histochemistry for the NOS isoforms and histochemistry for NOS activity and immunohistochemistry for protein nitration, brains were rapidly removed and hemisected. One hemisphere was immediately frozen in 2-methylbutane chilled on dry ice and stored at −80°C. The other hemisphere was submerged in 4% formaldehyde with 0.9% sodium chloride for 24 hours at 4°C, then cryoprotected in 30% sucrose in 0.1 M phosphate-buffered saline (PBS) and stored at 4°C. The fresh-frozen hemispheres were cut into 12-μm thick sections on a cryostat (Cryocut 1800; Cambridge Instruments, Bayreuth, Germany). These striatal sections (Bregma: +1.6 mm to +0.2 mm) were thaw-mounted on slides and stored at −20°C. Slides from all animals to be used for a particular in situ hybridization histochemical analysis were then postfixed in 4% formaldehyde/0.9% sodium chloride, acetylated in 0.25% acetic anhydride in 0.1 M triethanolamine/0.9% sodium chloride (pH, 8), dehydrated in alcohol, delipidated in chloroform, and rehydrated in a descending series of alcohol concentrations. Slides were air-dried and stored at −20°C until further processing. The fixed hemispheres were cut into 30-μm thick sections on a freezing microtome (Microm, HM 440E). These sections of striatum (Bregma: +1.6 mm to +0.2 mm) were stored at 4°C in 1 mg/ml sodium azide in 0.1 M PBS.

DAT Autoradiography. DAT levels in striatum were determined by [^{125}I]RTI-55 (PerkinElmer, Waltham, MA) binding, as previously described (Pastuzyn et al., 2012). Slides were apposed to film (Biomax MR; Eastman Kodak, Rochester, NY) for 24 hours and developed. Film autoradiograms were analyzed using NIH ImageJ (http://imagej.nih.gov/ij/) to yield mean background-subtracted gray values in the dorsomedial and dorsolateral striatum. Two rostral and two middle striatal sections were analyzed per rat and averaged. Mean gray values were then converted to percentage of control (Saline:Saline).

Nitrotyrosine Immunohistochemistry. Tissue sections from the fixed hemispheres were processed for nitrotyrosine immunohistochemistry. The sections were washed in 0.1 M PBS, incubated for 10 minutes in 0.1 M PBS with 3% hydrogen peroxide to block endogenous peroxidases, and washed again in 0.1 M PBS. The tissue was blocked with 0.1 M PBS containing 10% normal horse serum for 1 hour, then incubated overnight at 4°C with 5% normal horse serum and anti-nitrotyrosine mouse monoclonal antibody (1:100, Abcam, ab78163). The following day, sections were washed in 0.1 M PBS and incubated for 1 hour at room temperature with 5% normal horse serum and biotinylated horse anti-mouse IgG (1:200, Vector Laboratories, Burlingame, CA; BA-2001). Sections were then rinsed and incubated with avidin-biotinylated peroxidase complex (ABC Elite kit; Vector, PK-6100) for 1 hour at room temperature. The reaction was terminated by rinsing sections three times in 0.1 M PBS. The tissue was then incubated in nickel-enhanced diaminobenzidine tetrahydrochloride (Ni-DAB, Vector, SK-4100) for 3–5 minutes, washed again in 0.1 M PBS, mounted onto slides, dried, dehydrated, and coverslipped.

Images were digitized and densitometric analysis was performed with ImageJ, yielding mean gray values. Two rostral and two middle

striatal sections were analyzed per rat, and the values were averaged. Mean gray values were then compared among treatment groups.

nNOS, iNOS, and eNOS In Situ Hybridization Histochemistry. Full-length rat nNOS and iNOS cDNAs were generously provided by Dr. Michael Marletta (University of California Berkeley). Polymerase chain reaction amplification with forward and reverse primers containing T7 and SP6 promoter sequences were used to amplify the nNOS and iNOS cDNAs (nNOS antisense: 5′-AATACGACTCACTATAGGGCAGTTCATCATGTTCCCCGAT-3′; nNOS sense: 5′-ATTTAGGTGACACTATAGATGGAAGAGAACACGTTTGGGGT-3′; iNOS antisense: 5′-TAATACGACTCACTATAGGGACAATCCACAACTCGCTCCAA-3′; and iNOS sense 5′-ATTTAGGTGACACTATAGGTTCAGCTACGCCTTCAACACCA-3′). Ribonucleotide probes were then synthesized from the amplified cDNAs using T7 (antisense) or SP6 (sense) RNA polymerases (Roche Applied Science, Indianapolis, IN) and [^{35}S]-UTP (PerkinElmer Life and Analytical Sciences, Boston, MA). Full-length, rat eNOS cDNA in a pCMV-Sport6 vector was purchased from Origene (RN200806; Rockville, MD), transformed into *Escherichia coli* cells for amplification, and extracted using a DNA extraction kit (Qiagen, Valencia, CA). eNOS cDNA was then linearized with NcoI and transcribed with T7 (sense) and SP6 (antisense) RNA polymerases and [^{33}P]-UTP. For all in situ hybridizations, probes were prepared and added to hybridization buffer to a final concentration of 1×10^6 cpm/μl, as previously described (Keefe and Gerfen, 1996). Hybridization buffer (100 μl) with probe was applied to each slide containing four brain sections, each slide was covered with a glass coverslip, and slides were hybridized overnight in humid chambers at 55°C. The following day, slides were washed four times in 2 × saline-sodium citrate (0.15 M sodium chloride with 0.015 M sodium citrate), treated with Ribonuclease-A (5 mg/ml; Roche Applied Science) in 2 × SSC for 15 minutes at room temperature, washed again in 2 × SSC, dried, and apposed to X-ray film (Biomax MR; Eastman Kodak) for approximately 1 week.

Film autoradiograms were digitized and analyzed using ImageJ. The images of sections from all groups in an experiment that were processed and hybridized together were captured and measured under constant lighting and camera conditions. nNOS mRNA expression, which was punctate because of its expression in striatal interneurons (Kawaguchi et al., 1995), was quantified by counting the number of cells labeled for nNOS mRNA. To this end, images were thresholded to include cell bodies of nNOS-positive cells. The mean signal density per labeled cell was also measured from the thresholded images. For iNOS and eNOS mRNA expression, both of which were more diffuse, the mean gray value of the dorsal striatum was measured, and the mean gray value of the corpus callosum overlying the striatum was subtracted for background correction. Two rostral and two middle striatal sections were analyzed per rat and averaged.

The specificity of our iNOS probe was confirmed by examining the induction of iNOS mRNA in the brain of an animal infected with Theiler's murine virus, because previous studies have demonstrated an induction of iNOS in these animals (Oleszak et al., 1997; Iwahashi et al., 1999). As shown in Fig. 1A, hybridization of a brain section from this animal with the antisense ribonucleotide against iNOS revealed iNOS induction in the area of the intrahemispheric injection of the virus. Alternatively, hybridization of an adjacent brain section from the same animal with the sense ribonucleotide probe did not yield any staining (Fig. 1B). We also evaluated the specificity of our eNOS ribonucleotide probe. As shown in Fig. 1C, hybridization with the antisense ribonucleotide probe revealed expression in the pyramidal cell layer of the hippocampus, consistent with prior reports (Dinerman et al., 1994; Vaid et al., 1996; Doyle and Slater, 1997). In addition, hybridization of an adjacent brain section with the sense ribonucleotide probe again yielded no signal (Fig. 1D). Finally, the specificity of the nNOS antisense ribonucleotide probe used was based on the correspondence between the staining obtained in the present study and previous findings from our laboratory and others that showed the distribution of the nNOS/somatostatin/neuropeptide Y-containing interneuron population in striatum (Uhl and Sasek, 1986; Rushlow et al., 1995; Horner et al., 2006). Thus, the antisense ribonucleotide probes generated for this study appear to specifically label NOS isoform mRNAs in the brain.

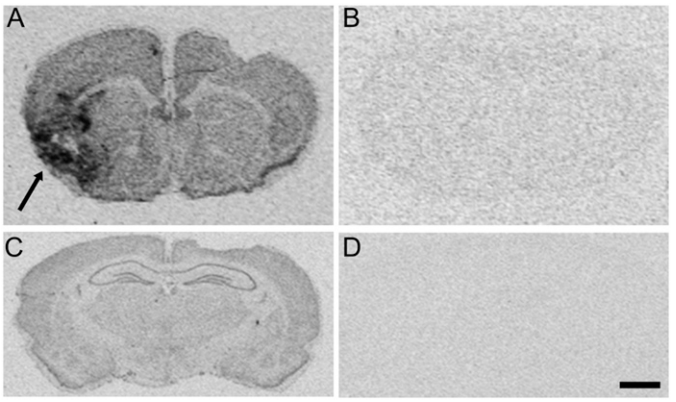

Fig. 1. Controls for iNOS and eNOS in situ hybridization histochemistry. (A) Positive control image of a striatal section from a mouse with Theiler's murine virus (TMV) infection in the brain (indicated by the arrow) showing detection of iNOS mRNA induction using the antisense ribonucleotide probe described in this article. (B) Negative control image showing a lack of signal in a brain section from the same TMV-infected mouse hybridized with the sense ribonucleotide probe. (C) Positive control image of a rat brain section at the level of the dorsal hippocampus hybridized with the antisense ribonucleotide probe against eNOS mRNA used in the present study. (D) Control image of a rat brain section at the level of the dorsal hippocampus hybridized with the sense ribonucleotide probe against eNOS mRNA used in the present study. Scale bar = 2 mm, applies to all panels.

NADPH Diaphorase Histochemical Staining. Tissue sections from the fixed hemispheres were processed for NADPH diaphorase histochemical staining to assess NOS activity (Hope et al., 1991). Tissue was washed in 0.1 M Tris-HCL (pH, 8.0), followed by preincubation in 0.1 M Tris-HCl containing 0.04% Tween-80 and 0.05% TritonX-100. The tissue was then incubated in Tris-HCl containing 0.8 mg/ml NADP, 0.16 mg/ml NBT, 0.04% Tween-80, 0.05% TritonX-100, 1 mM $MgCl_2$, and 15 mM malate for 2 hours at 37°C. Sections were then rinsed in 0.1 M Tris-HCL for 5 minutes, mounted onto slides, dried, and coverslipped. Digitized images of the NADPH diaphorase histochemical staining were captured under bright field conditions with a 40× objective with use of a Leica DM 4000B microscope. A 3 × 3 montage (0.63 mm^2) centered over dorsal striatum was captured from one hemisphere per section, resulting in four images per animal. The images were analyzed using ImageJ. Each image was thresholded such that the minimum threshold value in ImageJ was set to zero and the maximum threshold value was set to 16 points above the lowest edge of the threshold histogram. Blood vessels with NADPH diaphorase histochemical staining (indicative of eNOS activity) were excluded. The percentage area of the total remaining field with signal was measured and averaged across the four sections for each animal. This standardized image analysis allowed for the measurement of NADPH diaphorase-positive cell bodies and processes and excluded NADPH-diaphorase histochemical staining associated with endothelial cells. In addition, the number of cell bodies positive for NADPH diaphorase histochemical staining per image was recorded, averaged across the four sections for each animal, and then compared among treatment groups.

Statistical Analysis. All image analysis was conducted by an experimenter blinded to the treatment groups. Statistical analysis was performed using a two-factor analysis of variance [analysis of variance (ANOVA); PND60 treatment × PND90 treatment], followed by post hoc analysis via Student's t or Tukey HSD test, as appropriate. Statistical analysis of body temperature data was conducted using a multivariate ANOVA (MANOVA) with repeated measures (PND60 treatment × PND90 treatment × time), followed by post hoc analysis via t tests at individual time points to assess main effects of

treatments, as appropriate. No differences between dorsolateral and dorsomedial striatum were observed for the DAT binding, iNOS and eNOS mRNA expression, or nitrotyrosine staining; thus, values were averaged across these two regions for each striatal section.

Results

METH-Induced Hyperthermia in Rats Sacrificed 1 Hour After the Final Treatment on PND90. For the body temperature data collected during treatment of this cohort of animals on PND60 (Fig. 2A), MANOVA revealed a main effect of PND60 treatment ($F_{(1,33)}$=169.5, $P < 0.0001$) and time ($F_{(4,30)}$=49.5, $P < 0.0001$). There was also a significant PND60 treatment × time interaction ($F_{(4,30)}$=53.5, $P < 0.001$). Post hoc analysis revealed that the temperatures of animals receiving METH were significantly greater than those of controls at all four time points after the injections of METH began (60 minutes, t=16.3, $P < 0.0001$; 180 minutes, t=15.5, $P < 0.0001$; 300 minutes, t=9.4, $P < 0.0001$; 420 minutes, t=9.7, $P < 0.0001$), but were not different from controls at baseline (t=1.6, $P = 0.1$).

For the body temperature data collected during treatment of this cohort of animals on PND90 (Fig. 2B), MANOVA revealed a main effect of PND90 treatment ($F_{(1,31)}$=343.3, $P < 0.0001$), a main effect of time ($F_{(3,29)}$=33.9, $P < 0.0001$), and significant PND60 treatment × time ($F_{(3,29)}$=5.2, $P = 0.005$) and PND90 treatment × time ($F_{(3,29)}$=51.4, $P < 0.0001$) interactions. Post hoc analysis of the PND60 × time interaction revealed that, at baseline on PND90, the rats treated with METH at PND60 had statistically higher body temperatures than did rats treated with saline on PND60 (t=4.1, $P = 0.0002$). However, the body temperatures at the

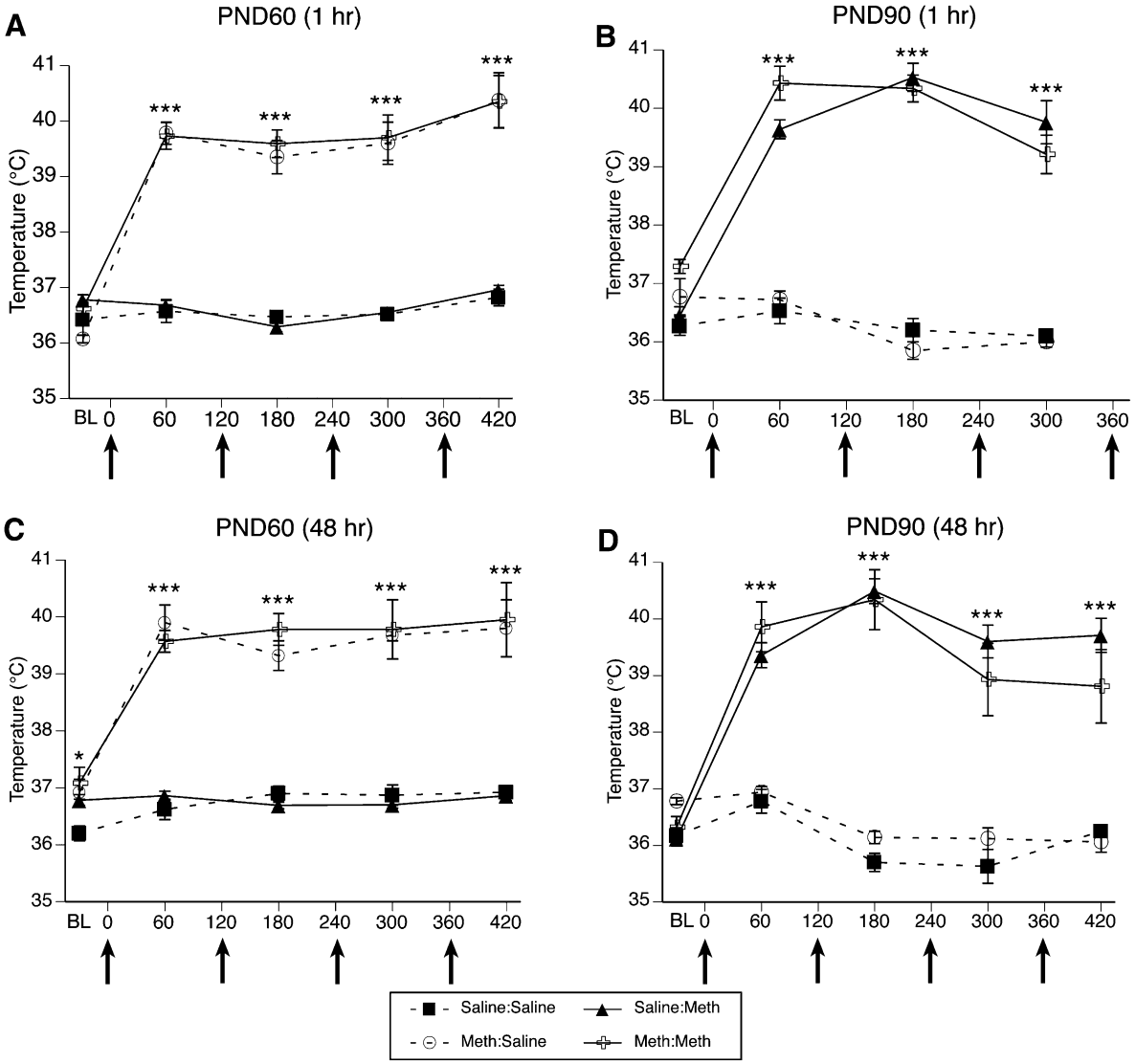

Fig. 2. Core body temperatures (mean ± S.E.M.; n = 5–12) of animals that received systemic injections of saline (4 × 1 mL/kg, subcutaneous at 2-hour intervals) or METH (4 × 10 mg/kg, subcutaneous at 2-hour intervals). Treatment group designations in the legend indicate PND60 treatment:PND90 treatment, resulting in the four treatment groups. Rectal temperatures were obtained 30 minutes before the first injection [baseline (BL)] and 1 hour after each subsequent injection. *X*-axis values represent minutes after the first injection, and arrows represent the time of each saline or METH injection. (A and C) Temperatures recorded during treatment on PND60 of animals sacrificed 1 hour (A) or 48 hours (C) after the last injection on PND90. (B and D) Temperatures recorded during treatment on PND90 of animals sacrificed 1 hour (B) or 48 hours (D) after the last injection on PND90. *$P < 0.05$; ***$P < 0.001$ indicate that groups receiving METH were significantly hyperthermic, relative to groups receiving saline.

other time points recorded on PND90 were not different between the rats treated with METH versus saline at PND60 (60 minutes, t=1.1, $P = 0.3$; 180 minutes, t=0.2, $P = 0.8$; 300 minutes, t=0.5, $P = 0.6$). Post hoc analysis of the PND90 treatment × time interaction again revealed that the temperatures of animals acutely receiving METH (i.e., PND90 treatment) were significantly higher than those of controls at all time points after the administration of METH began (60 minutes, t=12.3, $P < 0.0001$; 180 minutes, t=17.9, $P < 0.0001$; 300 minutes, t=9.7, $P < 0.0001$), but were not different from controls at baseline (t=1.7, $P = 0.1$). Of importance, there was no significant PND60 treatment × PND90 treatment interaction ($F_{(1,31)}=0.3$, $P = 0.6$) or PND60 treatment × PND90 treatment × time interactions ($F_{(3,29)}=0.6$, $P = 0.6$), indicating that the pretreatment on PND60 did not impact METH-induced hyperthermia on PND90.

METH-Induced Hyperthermia in Rats Sacrificed 48 Hours After the Final Treatment on PND90. For the body temperature data collected during treatment of this cohort of animals on PND60 (Fig. 2C), MANOVA revealed a main effect of PND60 treatment ($F_{(1,26)}=213$, $P < 0.0001$), a main effect of time ($F_{(4,23)}=52.8$, $P < 0.0001$), and a significant PND60 treatment × time interaction ($F_{(4,23)}=33.8$, $P < 0.0001$). Post hoc analysis revealed that the body temperatures of the rats given METH at PND60 were significantly greater than the temperatures of the controls at all time points (baseline, t=2.5, $P = 0.02$; 60 minutes, t=15.9, $P < 0.0001$; 180 minutes, t=14.2 $P < 0.0001$; 300 minutes, t=10.8, $P < 0.0001$; 420 minutes, t=8.1, $P < 0.0001$).

For the body temperature data collected during treatment of this cohort of animals on PND90 (Fig. 2D), MANOVA revealed a main effect of PND90 treatment ($F_{(1,24)}=195.1$, $P < 0.0001$), a main effect of time ($F_{(4,21)}=35.7$, $P < 0.0001$), and a significant PND90 treatment × time interaction ($F_{(4,21)}=51.4$, $P < 0.0001$). Post hoc analysis of the PND90 treatment × time interaction again revealed that the temperatures of animals acutely receiving METH (i.e., PND90 treatment) were significantly higher than those of controls at all time points after the administration of METH began (60 minutes, t=10.8, $P < 0.0001$; 180 minutes, t=16.9, $P < 0.0001$; 300 minutes, t=9.4, $P < 0.0001$; 420 minutes, t=9.1, $P < 0.0001$), but were not different from controls at baseline (t=1.2, $P = 0.3$). Of importance, there was no significant PND60 treatment × PND90 treatment interaction ($F_{(1,24)}=1.7$, $P = 0.2$), PND60 treatment × time ($F_{(4,21)}=1.6$, $P = 0.2$), or PND60 treatment × PND90 treatment × time interaction ($F_{(4,21)}=1.3$, $P = 0.3$), indicating again that the pretreatment on PND60 did not impact METH-induced hyperthermia on PND90.

METH-Induced DA Depletions. Administration of METH resulted in significant decreases in [^{125}I]RTI-55 binding to the DAT, compared with saline-treated controls (Fig. 3). In animals sacrificed 1 hour after the last injection on PND90 (Fig. 3A), a two-factor ANOVA revealed a main effect of PND60 treatment ($F_{(1,30)}=42.1$, $P < 0.0001$), with rats treated with METH at PND60 showing decreased DAT binding, compared with rats treated with saline. There was no significant main effect of PND90 treatment ($F_{(1,30)}=79.3$, $P = 0.6$) and no significant PND60 treatment × PND90 treatment interaction ($F_{(1,30)}=0.1$, $P = 0.8$). In the cohort of animals sacrificed 48 hours after the last injection on PND90 (Fig. 3, B and C), a two-factor ANOVA revealed a main effect of PND60 treatment ($F_{(1,23)}=11.2$, $P < 0.003$), a main effect of PND90 treatment ($F_{(1,23)}=202.2$, $P < 0.0001$), and a significant PND60 treatment × PND90 treatment interaction ($F_{(1,23)}=78.9$, $P < 0.0001$). Post hoc analysis of the interaction revealed that all treatment groups were significantly different from each other (Tukey's test, P values ≤ 0.005).

To assess whether the decrease in DAT autoradiographic labeling reflects METH-induced DA terminal degeneration, we examined, in another cohort of animals treated with the same neurotoxic regimen of METH, the relation between this measure and other indices of METH-induced DA depletion. [^{125}I]RTI-55 binding to the DAT correlates strongly with decreases in DA tissue content measured via high-performance liquid chromatography ($n = 9$; DM $r^2=0.897$, $P < 0.0001$, DL $r^2=0.79$, $P = 0.0013$). Thus, [^{125}I]RTI-55 binding to the DAT appears to reflect the degree of DA loss induced by the neurotoxic regimen of METH.

Effect of METH on Protein Nitration in Striatum. Consistent with prior reports in the literature implicating reactive nitrogen species in METH-induced neurotoxicity (Di Monte et al., 1996; Itzhak and Ali, 1996; Imam et al., 1999), in this study, treatment of rats with a neurotoxic regimen of METH resulted in a significant increase in protein nitration in the striata of rats sacrificed 1 hour after the final injection on PND90 (Fig. 4). A two-factor ANOVA revealed a significant main effect of PND90 treatment ($F_{(1,31)}= 8.8$, $P = 0.006$), but no main effect of PND60 treatment ($F_{(1,31)}=0.1$, $P = 0.7$) and no significant PND60 treatment × PND90 treatment interaction ($F_{(1,31)}=0.3$, $P = 0.6$). Thus, all rats receiving a neurotoxic regimen of METH on PND90 (i.e., Saline:METH and METH:METH groups), whether they experienced acute toxicity or not, showed equivalent increases in protein nitration in striatum.

Effect of METH on iNOS Expression in Striatum. Repeated high-dose administrations of METH did not result in an induction of iNOS mRNA expression either at 1 hour (Fig. 5A) or 48 hours (Fig. 5, B and C) after the last injection on PND90. A two-way ANOVA on iNOS expression in the striata of rats sacrificed 1 hour after the final injection on PND90 revealed no significant main effects of PND60 treatment ($F_{(1,30)}=0.0002$, $P = 0.99$) or PND90 treatment ($F_{(1,30)}=0.3$, $P = 0.6$) and no significant PND60 treatment × PND90 treatment interaction ($F_{(1,30)}=0.0000$, $P = 0.99$). Similarly, analysis of iNOS expression in the striata of animals sacrificed 48 hours after the last injection on PND90 showed no significant main effects of PND60 treatment ($F_{(1,23)}=0.9$, $P = 0.3$) or PND90 treatment ($F_{(1,23)}=0.04$, $P = 0.8$) and no significant PND60 treatment × PND90 treatment interaction ($F_{(1,23)}=0.1$, $P = 0.7$).

Effect of METH on eNOS Expression in Striatum. Administration of the neurotoxic regimen of METH did not alter eNOS mRNA expression in the striata of rats sacrificed either at 1 hour (Fig. 6A) or at 48 hours (Fig. 6, B and C) after the last administration of METH on PND90. That is, in the cohort of rats sacrificed at 1 hour after the last injection, there was no significant main effect of PND60 treatment ($F_{(1,31)}=0.6$, $P = 0.5$) or PND90 treatment ($F_{(1,31)}=0.7$, $P = 0.4$) and no significant PND60 treatment × PND90 treatment interaction ($F_{(1,31)}=0.3$, $P = 0.6$). Likewise, in the cohort of rats sacrificed 48 hours after the last injection, there was no significant main effect of PND60 treatment ($F_{(1,23)}=1.3$, $P = 0.3$) or PND90 treatment

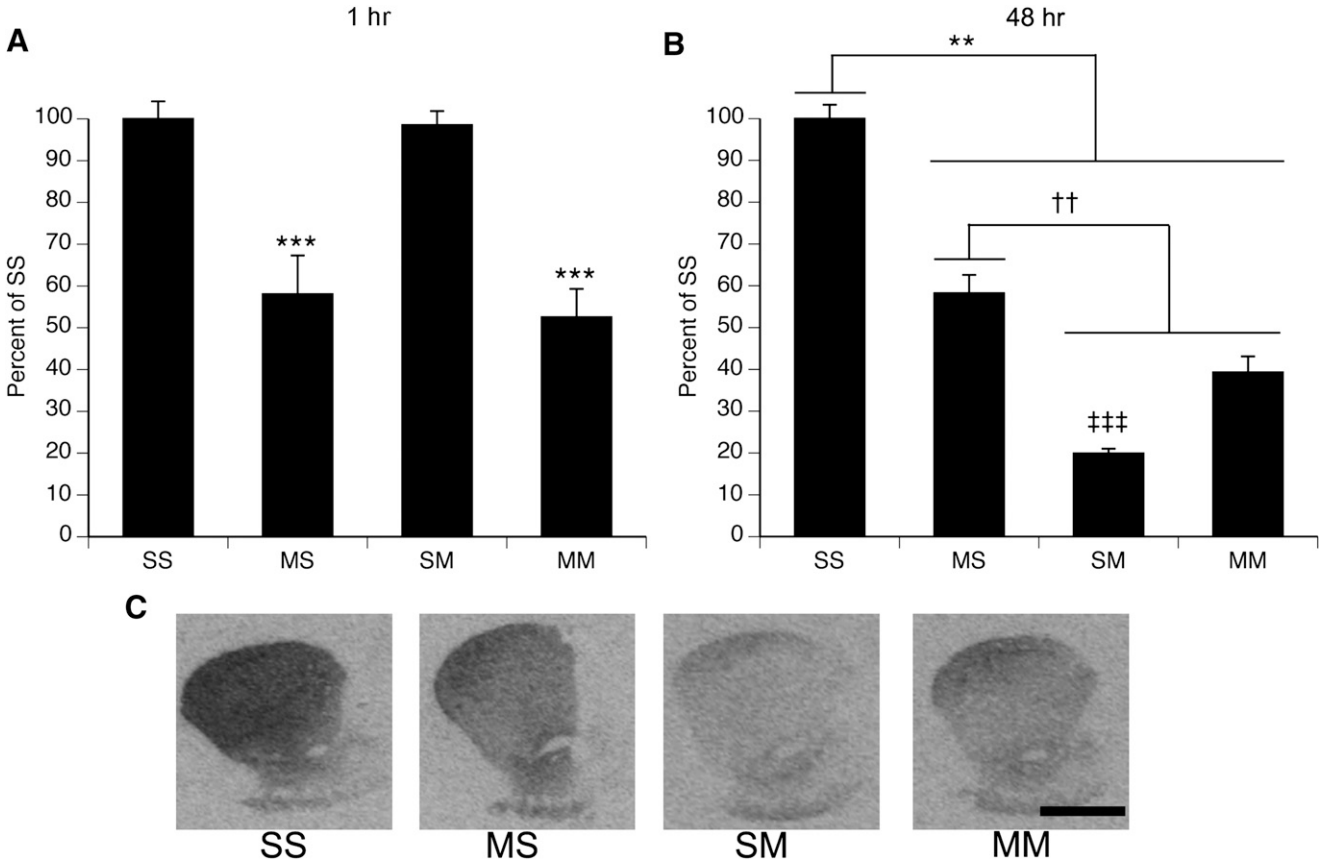

Fig. 3. Striatal DAT binding density after single or repeated exposure to a neurotoxic regimen of METH (mean ± S.E.M.; n = 5–12). Treatment group designations indicate PND60 treatment:PND90 treatment, resulting in the four treatment groups: Saline:Saline (SS), METH:Saline (MS), Saline:METH (SM), and METH:METH (MM). (A) Animals sacrificed 1 hour after the last injection on PND90. ***Main effect of PND60 treatment, $P < 0.001$. (B) Animals sacrificed 48 hours after the last injection on PND90. **SS group significantly different from all other groups, $P < 0.005$; ††MS group significantly different from all other groups; $P < 0.005$; ‡‡‡SM group significantly different from all other groups, $P < 0.005$. (C) Representative images of DAT autoradiography in animals sacrificed 48 hours after the last injection. Scale bar = 2 mm, applies to all images.

($F_{(1,23)}$=0.4, P = 0.6) and no significant PND60 treatment × PND90 treatment interaction ($F_{(1,23)}$=0.8, P = 0.4).

Effect of METH on nNOS Expression in Striatum. Repeated high-dose administrations of METH did not alter the number of cells expressing nNOS mRNA (Fig. 7A) or the mean density of nNOS mRNA signal per cell (Fig. 7B) in rats sacrificed either 1 hour or 48 hours after the last injection on PND90. That is, there was no main effect of PND60 treatment (1-hour survival cohort, $F_{(1,30)}$=0.4, P = 0.5; 48-hour survival cohort, $F_{(1,23)}$=0.3, P = 0.8), no main effect of PND90 treatment (1-hour survival cohort, $F_{(1,30)}$=0.1, P = 0.7; 48-hour survival cohort, $F_{(1,23)}$=0.0003, P = 0.99), and no significant PND60 treatment × PND90 treatment interaction (1-hour survival cohort, $F_{(1,30)}$=0.003, P = 0.96; 48-hour survival cohort, $F_{(1,23)}$=0.3, P = 0.6) on the number of nNOS-positive cells in each striatum . Likewise, there was no main effect of PND60 treatment (1-hour survival cohort, $F_{(1,30)}$=0.02, P = 0.9; 48-hour survival cohort, $F_{(1,23)}$=0.3, P = 0.6), no main effect of PND90 treatment (1-hour survival cohort, $F_{(1,30)}$=0.5, P = 0.5; 48-hour survival cohort, $F_{(1,23)}$=3.1, P = 0.09), and no significant PND60 treatment × PND90 treatment interaction (1-hour survival cohort, $F_{(1,30)}$=0.7, P = 0.4; 48-hour survival cohort, $F_{(1,23)}$=2.8, P = 0.1) on the mean density of nNOS mRNA staining per cell.

To further validate the nNOS mRNA results, we quantified the number of NADPH diaphorase-positive cells in the striata of animals sacrificed at 1 hour after the last injection. These data confirmed that the number of NADPH diphaorase-positive cells did not change after single or repeated exposure to a neurotoxic regimen of METH (unpublished data).

Effect of METH on NOS Activity in the Striatum. Because eNOS and nNOS are constitutively expressed, the enzymes increase their production of NO without observable changes in mRNA expression. Previous work has shown that the NADPH diaphorase histochemical staining allows for the quantification of nNOS activity in the striatum (Dawson et al., 1991; Hope et al., 1991; Morris et al., 1997). Therefore, we examined the effects of a neurotoxic regimen of METH on NOS activity, as reflected in NADPH diaphorase histochemical staining in striatum. Administration of the METH binge regimen on PND90 resulted in a significant increase in NADPH diaphorase histochemical staining in the striata of rats sacrificed 1 hour after the final injection on PND90 (Fig. 8). A two-factor ANOVA revealed a main effect of PND90 treatment ($F_{(1,28)}$=5.8, $P < 0.05$), but no main effect of PND60 treatment ($F_{(1,28)}$=0.06, P = 0.8) and no significant PND60 treatment × PND90 treatment interaction ($F_{(1,28)}$=0.9, P = 0.4). Thus, as was the case for protein nitration in striatum, NADPH diaphorase histochemical staining and, thus, nNOS

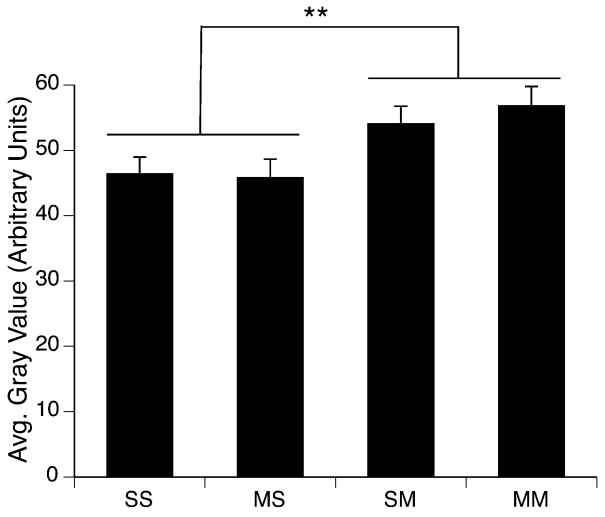

Fig. 4. Quantitative analysis of the effects of single or repeated METH exposure on protein nitration in the striata of animals sacrificed 1 hour after the last injection on PND90. Protein nitration data are expressed as average (avg.) gray values (mean ± S.E.M.; n = 6–12) obtained from densitometric analysis of immunohistochemically stained sections. Treatment group designations indicate PND60 treatment:PND90 treatment, resulting in the four treatment groups: Saline:Saline (SS), METH:Saline (MS), Saline:METH (SM), and METH:METH (MM). **Significant main effect of PND90 treatment, $P < 0.01$.

activity were increased in all rats receiving a neurotoxic regimen of METH on PND90, regardless of whether they experienced acute DA neuron toxicity (Saline:METH group) or not (METH:METH group).

Discussion

Recent data suggest that abuse of METH may contribute to increased incidence of Parkinsonism secondary to damage to striatal DA systems (Callaghan et al., 2012). Thus, delineating the necessary and sufficient factors involved in METH-induced damage to central DA systems is critical for advancing our ability to mitigate long-term consequences of METH use. Our laboratory and others have found that animals pretreated with a neurotoxic regimen of METH do not show further depletions of striatal DA when challenged with a subsequent neurotoxic regimen of METH (Thomas and Kuhn, 2005; Hanson et al., 2009). This paradigm thus affords a model in which animals can be matched for acute METH exposure, but differentiated with respect to acute DA neuron toxicity, to identify factors that are sufficient to induce striatal DA toxicity. Prior evidence has suggested that NO may be such a critical factor for METH-induced neurotoxicity (Di Monte et al., 1996; Itzhak and Ali, 1996; Deng and Cadet, 1999; Imam et al., 1999). Therefore, the purpose of this study was to determine whether NO production secondary to METH exposure is sufficient to induce striatal DA depletions and to determine the source of NO after METH exposure. The data reveal that production of NO, as reflected in protein nitration, is similar whether an animal is experiencing acute DA toxicity or not, suggesting that NO production is not sufficient to induce such toxicity. Furthermore, the data suggest that the NO likely arises from the constitutively expressed isoforms of NOS, most likely the nNOS-containing interneuron population in striatum.

The present results suggest that NO production in response to METH may not contribute to METH-induced DA neuron toxicity, because both rats experiencing acute toxicity to METH administration on PND90 and those resistant to it showed equivalent increases in protein nitration and NOS activity in striatum. As noted above, studies have implicated NO in METH-induced DA neuron toxicity on the basis of observations that inhibition of NOS blocks or attenuates such toxicity (Di Monte et al., 1996; Itzhak and Ali, 1996; Ali and Itzhak, 1998; Itzhak et al., 1998; Imam et al., 1999; Itzhak et al., 2000a; Itzhak et al., 2000b; Itzhak et al., 2004). However, there is controversy over whether this protection reflects a critical mechanistic role of NO in METH-induced DA neuron toxicity or whether it results from a disruption of METH-induced hyperthermia necessary for the toxicity (Taraska and Finnegan, 1997; Callahan and Ricaurte,

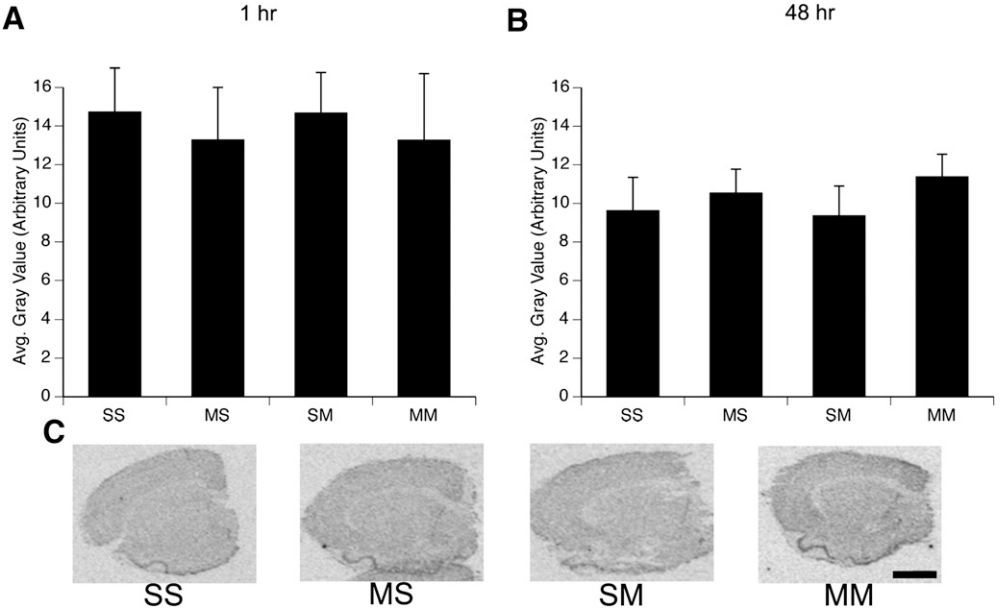

Fig. 5. Quantitative analysis of the effects of single or repeated METH exposure on iNOS mRNA expression in the striata of animals sacrificed 1 hour (A) or 48 hour (B) after the last injection on PND90. Treatment group designations indicate PND60 treatment:PND90 treatment, resulting in the four treatment groups: Saline:Saline (SS), METH:Saline (MS), Saline:METH (SM), and METH:METH (MM). Values are background-subtracted average (avg.) gray values (mean ± SEM; n = 5-12). No significant differences between treatment groups were observed. (C) Representative images of iNOS mRNA in situ hybridization histochemical staining in rats sacrificed 48 hour after the last injection on PND90. Scale bar = 2 mm, applies to all images.

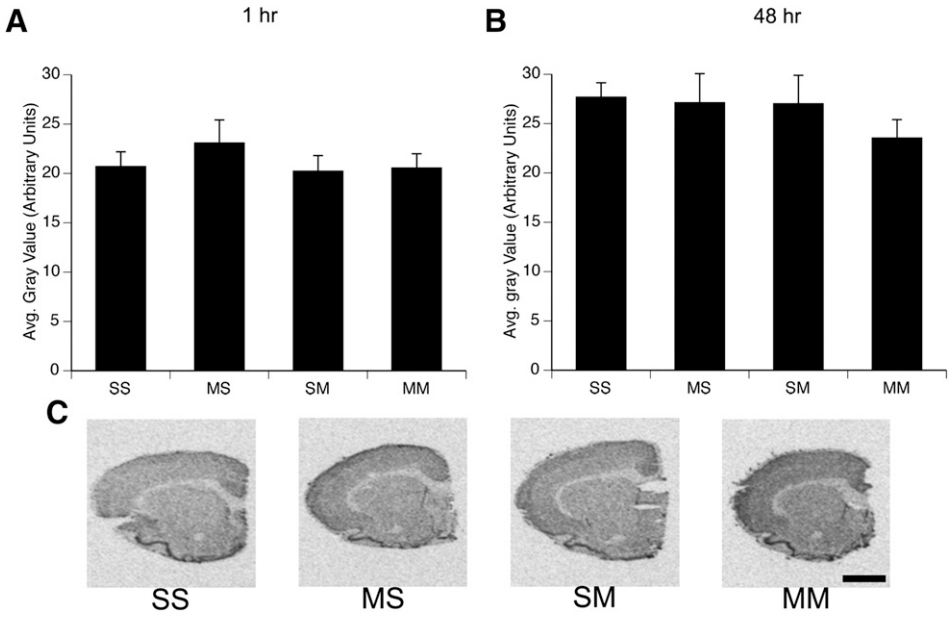

Fig. 6. Quantitative analysis of the effects of single or repeated METH exposure on eNOS mRNA expression in the striata of animals sacrificed 1 hour (A) or 48 hours (B) after the last injection on PND90. Treatment group designations indicate PND60 treatment:PND90 treatment, resulting in the four treatment groups: Saline:Saline (SS), METH:Saline (MS), Saline:METH (SM), and METH:METH (MM). Values are background-subtracted mean gray values (mean ± S.E.M.; n = 5–12). No significant differences between treatment groups were observed. (C) Representative images of eNOS mRNA in situ hybridization histochemical staining in rats sacrificed 48 hours after the last injection on PND90. Scale bar = 2 mm, applies to all images.

1998). The present findings of a dissociation between indices of NO production and acute DA neuron toxicity support the conclusion that the generation of NO is not sufficient for METH-induced DA toxicity.

Although the present data suggest that generation of NO is not sufficient for METH-induced DA terminal damage, we cannot rule out the possibility that NO is necessary for such toxicity when it occurs (e.g., in the Saline:METH group), because NO may act in concert with other factors under those conditions to contribute to the toxicity. For example, evidence suggests that NO regulates DA release in striatum (Zhu and Luo, 1992; West and Galloway, 1997; West et al., 2002), including METH-induced DA release (Bowyer et al., 1995; Inoue et al., 1996), which has been suggested to play an important role in damage to DA terminals (O'Dell et al., 1991; O'Dell et al., 1993; Gross et al., 2011). Thus, NO production during an initial exposure to a neurotoxic regimen of METH may increase DA overflow, and this DA overflow may result in the DA neuron toxicity. Under conditions in which DA overflow is reduced, such as in animals with prior METH-induced DA neuron toxicity (Hanson et al., 2009), such a role of NO might not be apparent. Clearly, studies with strict control over potential contributing factors allowing for systematic independent and coordinate manipulation of the factors will be necessary to fully understand the process by which METH induces DA neurotoxicity. Furthermore, we cannot exclude a role of NO in striatal-efferent neuron toxicity observed in some models of METH-induced neurotoxicity (Zhu et al., 2009).

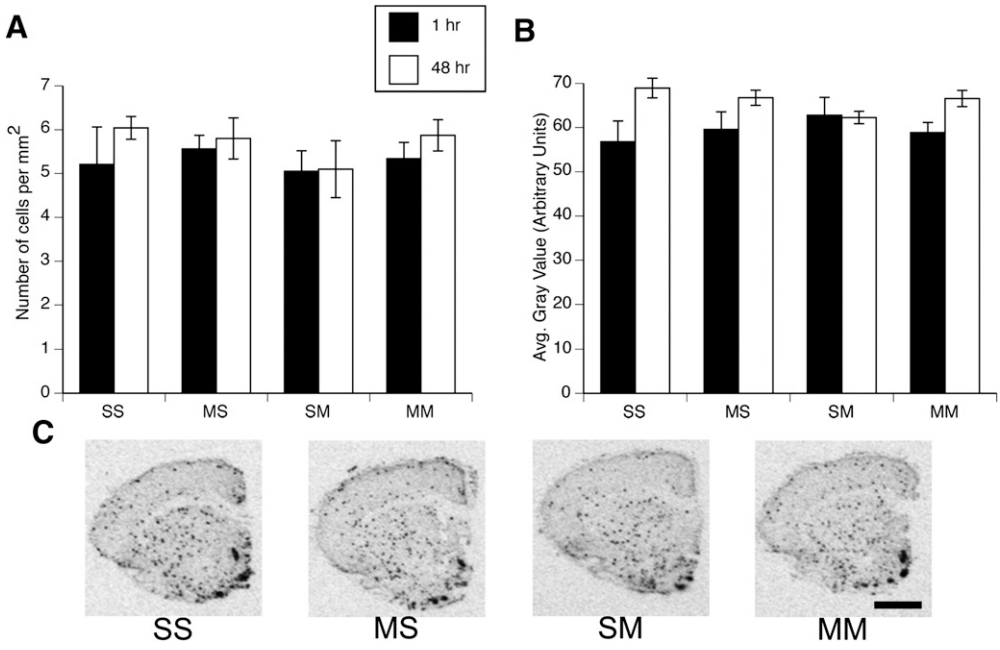

Fig. 7. Quantitative analysis of the effects of single or repeated METH exposure on nNOS mRNA expression in the striata of animals sacrificed 1 hour or 48 hours after the last injection on PND90. Treatment group designations indicate PND60 treatment:PND90 treatment, resulting in the four treatment groups: Saline:Saline (SS), METH:Saline (MS), Saline:METH (SM), and METH:METH (MM). Values are expressed as the mean number of cells expressing nNOS per square millimeter of the imaged striatal sections (A; mean ± S.E.M.; n = 4–12) and the mean density (i.e., average [avg.] gray value) of the nNOS signal per labeled cell (B) in the striatal sections analyzed. No significant differences among treatment groups were observed. (C) Representative images of nNOS mRNA in situ hybridization histochemical staining in rats sacrificed 48 hours after the last injection on PND90. Scale bar = 2 mm, applies to all images.

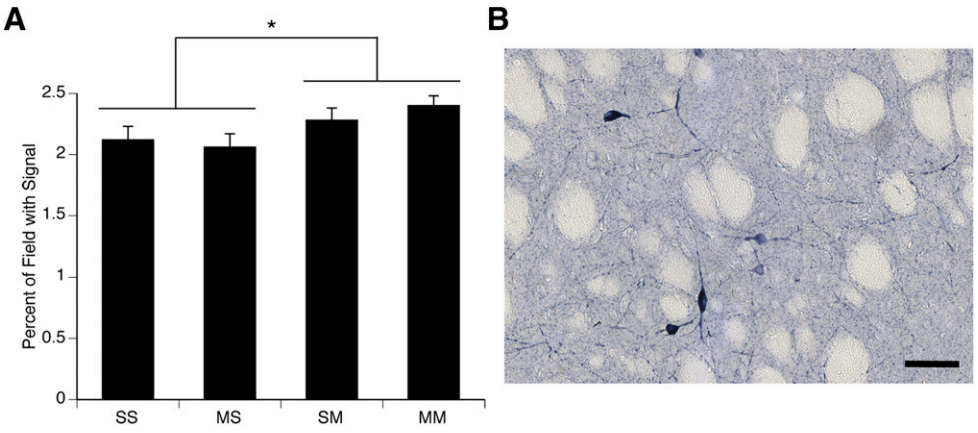

Fig. 8. (A) Quantitative analysis of the effects of single or repeated METH exposure on nNOS activity in the striata of animals sacrificed 1 hour after the last injection on PND90. Treatment group designations indicate PND60 treatment:PND90 treatment, resulting in the four treatment groups: Saline:Saline (SS), METH:Saline (MS), Saline:METH (SM), and METH:METH (MM). Data are expressed as the percentage area of the field with signal above threshold. *Significant main effect of PND90 treatment, $P < 0.05$. (B) Representative image of NADPH diaphorase histochemical staining in an SM animal sacrificed 1 hour after the last injection on PND90. Scale bar = 50μm.

Although the necessity of NO for METH-induced DA neurotoxicity remains in question, it is clear from the present findings that administration of a binge regimen of METH increases NO production. The data further suggest that METH-induced increases in NOS activity/NO production may largely arise secondary to activation of nNOS, which is found in striatal somatostatin/neuropeptide Y-positive interneurons (Kawaguchi et al., 1995). First, we found no induction of iNOS mRNA 1 or 48 hours after the last administration on PND90. These data are consistent with previous work (Deng and Cadet, 1999) showing that iNOS protein expression is not induced after a neurotoxic regimen of METH. However, in that study, iNOS protein was examined at 1 hour, 24 hours, and 1 week after exposure to METH, time points when glial cells may not be fully activated (LaVoie et al., 2004). Of importance, it is these cell types in which induction of iNOS mRNA expression typically occurs (Gibson et al., 2005). Therefore, we examined iNOS expression at 1 and 48 hours, because previous work has shown that glial reactivity peaks at 48 hours after a neurotoxic regimen of METH (LaVoie et al., 2004). Our data combined with the work of others (Deng and Cadet, 1999) strongly suggest that iNOS is not a likely source of NO after METH exposure.

Second, induction of eNOS and nNOS isoforms also does not appear to underlie the METH-induced increases in NO production. At both 1 and 48 hours after the last administration of METH on PND90, there were no changes in the numbers of cells expressing eNOS or nNOS mRNA. Likewise, there was no increase in the numbers of NADPH diaphorase-positive cells and no increase in eNOS immunohistochemical staining in sections from animals sacrificed 48 hours after the last injection (data not shown). A prior study in mice reported an increase in the number of cells expressing nNOS protein after a neurotoxic regimen of METH (Deng and Cadet, 1999), but others have not (Wang et al., 2008; Wang and Angulo, 2011). Differences in nNOS expression have been observed between species and strains of animals within a species (Blackshaw et al., 2003), suggesting that differences between our results and the prior report by Deng and Cadet may reflect a species difference. Our data thus suggest that induction of eNOS or nNOS expression by METH exposure is not contributing to METH-induced NO production in this rat model.

Taken together, the data suggest that activation of constitutively expressed NOS isoforms (i.e., eNOS or nNOS) is the likely basis for METH-induced NO production. This conclusion is based on the data showing increased NADPH diaphorase histochemical staining, which reflects NOS activity (Hope et al., 1991). We further restricted this assay to determination of nNOS activity in striatum by excluding stained vasculature from the images during the analysis and thresholding the images to include only cell bodies and processes of NADPH-positive cells. We found that animals acutely exposed to a neurotoxic regimen of METH on PND90 showed increased staining, suggesting increased nNOS activation by the binge regimen of METH. On the basis of these observations, we conclude that activation of nNOS is a major source of NO production in response to the binge regimen of METH. However, we cannot rule out a contribution of eNOS activation to METH-induced NO production and METH-induced protein nitration in striatum.

Activation of nNOS in striatal interneurons in the context of binge regimens of METH is not surprising, because of what is known about NO production in striatum and the cascade of events occurring during and after METH administration. First, activation of the *N*-methyl-D-aspartate (NMDA) subtype of glutamate (GLU) receptors initiates NO production via Ca-dependent activation of nNOS (Garthwaite et al., 1988; Bredt and Snyder, 1989). Furthermore, binge regimens of METH increase GLU efflux in striatum and activation of NMDA receptors (Nash and Yamamoto, 1992; Mark et al., 2004). Second, activation of DA D1 receptors increases NO efflux in striatum (Le Moine et al., 1991; Sammut et al., 2006) and NADPH diaphorase histochemical staining (Morris et al., 1997; Hoque et al., 2010), and striatal nNOS-containing interneurons express DA D1 family receptors (Le Moine et al., 1991). Furthermore, NMDA and DA D1 receptor activation work in concert to increase NO production (Park and West, 2009), and stimulation of either type of receptor or blockade of either type of receptor decreases NOS activity, as assessed via NADPH diaphorase histochemical staining (Morris et al., 1997). Together with data showing increased extracellular levels of both DA and GLU during and after METH exposure (O'Dell et al., 1991; Nash and Yamamoto, 1992; O'Dell et al., 1993), it seems to be likely that activation of nNOS in striatal interneurons is a major source of NO production after METH exposure.

In conclusion, the data presented here show that administration of a binge regimen of METH in rats increases protein nitration in striatum. The data further show that activation of

nNOS, as reflected in increased NADPH-diaphorase histochemical staining in cell bodies and processes of striatal interneurons, was apparent in rats acutely exposed to a binge regimen of METH, implicating nNOS as the likely source of METH-induced NO production. However, the data also show a dissociation between measures of NOS activity (NADPH diaphorase staining) and NO production (immunohistochemical staining of protein nitration) and METH-induced DA neurotoxicity, suggesting that NO production by a binge regimen of METH is not sufficient to induce acute DA neurotoxicity and that NO may not be a useful therapeutic target for prevention of acute METH-induced neurotoxicity in human METH abusers.

Acknowledgments

The authors thank Dr. Michael Marletta for the nNOS and iNOS cDNAs, and Dr. Steve O'Dell in Dr. John Marshall's laboratory for assistance with the DAT autoradiography assay.

Author Contributions

Participated in research design: Friend, Son, Fricks-Gleason, Keefe.

Conducted experiments: Friend, Son, Fricks-Gleason.

Performed data analysis: Friend, Son, Fricks-Gleason, Keefe.

Wrote or contributed to the writing of the manuscript: Friend, Son, Fricks-Gleason, Keefe.

References

Ali SF and Itzhak Y (1998) Effects of 7-nitroindazole, an NOS inhibitor on methamphetamine-induced dopaminergic and serotonergic neurotoxicity in mice. *Ann N Y Acad Sci* **844**:122–130.

Ali SF, Newport GD, Holson RR, Slikker W, Jr, and Bowyer JF (1994) Low environmental temperatures or pharmacologic agents that produce hypothermia decrease methamphetamine neurotoxicity in mice. *Brain Res* **658**:33–38.

Anderson KL and Itzhak Y (2006) Methamphetamine-induced selective dopaminergic neurotoxicity is accompanied by an increase in striatal nitrate in the mouse. *Ann N Y Acad Sci* **1074**:225–233.

Blackshaw S, Eliasson MJ, Sawa A, Watkins CC, Krug D, Gupta A, Arai T, Ferrante RJ, and Snyder SH (2003) Species, strain and developmental variations in hippocampal neuronal and endothelial nitric oxide synthase clarify discrepancies in nitric oxide-dependent synaptic plasticity. *Neuroscience* **119**:979–990.

Bowyer JF, Clausing P, Gough B, Slikker W, Jr, and Holson RR (1995) Nitric oxide regulation of methamphetamine-induced dopamine release in caudate/putamen. *Brain Res* **699**:62–70.

Bredt DS and Snyder SH (1989) Nitric oxide mediates glutamate-linked enhancement of cGMP levels in the cerebellum. *Proc Natl Acad Sci USA* **86**:9030–9033.

Callaghan RC, Cunningham JK, Sykes J, and Kish SJ (2012) Increased risk of Parkinson's disease in individuals hospitalized with conditions related to the use of methamphetamine or other amphetamine-type drugs. *Drug Alcohol Depend* **120**: 35–40.

Callahan BT and Ricaurte GA (1998) Effect of 7-nitroindazole on body temperature and methamphetamine-induced dopamine toxicity. *Neuroreport* **9**:2691–2695.

Dawson TM, Bredt DS, Fotuhi M, Hwang PM, and Snyder SH (1991) Nitric oxide synthase and neuronal NADPH diaphorase are identical in brain and peripheral tissues. *Proc Natl Acad Sci USA* **88**:7797–7801.

Deng X and Cadet JL (1999) Methamphetamine administration causes overexpression of nNOS in the mouse striatum. *Brain Res* **851**:254–257.

Di Monte DA, Royland JE, Jakowec MW, and Langston JW (1996) Role of nitric oxide in methamphetamine neurotoxicity: protection by 7-nitroindazole, an inhibitor of neuronal nitric oxide synthase. *J Neurochem* **67**:2443–2450.

Dinerman JL, Dawson TM, Schell MJ, Snowman A, and Snyder SH (1994) Endothelial nitric oxide synthase localized to hippocampal pyramidal cells: implications for synaptic plasticity. *Proc Natl Acad Sci USA* **91**:4214–4218.

Doyle CA and Slater P (1997) Localization of neuronal and endothelial nitric oxide synthase isoforms in human hippocampus. *Neuroscience* **76**:387–395.

Garthwaite J, Charles SL, and Chess-Williams R (1988) Endothelium-derived relaxing factor release on activation of NMDA receptors suggests role as intercellular messenger in the brain. *Nature* **336**:385–388.

Gibson CL, Coughlan TC, and Murphy SP (2005) Glial nitric oxide and ischemia. *Glia* **50**:417–426.

Gross NB, Duncker PC, and Marshall JF (2011) Striatal dopamine D1 and D2 receptors: widespread influences on methamphetamine-induced dopamine and serotonin neurotoxicity. *Synapse* **65**:1144–1155.

Guilarte TR, Nihei MK, McGlothan JL, and Howard AS (2003) Methamphetamine-induced deficits of brain monoaminergic neuronal markers: distal axotomy or neuronal plasticity. *Neuroscience* **122**:499–513.

Hanson JE, Birdsall E, Seferian KS, Crosby MA, Keefe KA, Gibb JW, Hanson GR, and Fleckenstein AE (2009) Methamphetamine-induced dopaminergic deficits and refractoriness to subsequent treatment. *Eur J Pharmacol* **607**:68–73.

Hope BT, Michael GJ, Knigge KM, and Vincent SR (1991) Neuronal NADPH diaphorase is a nitric oxide synthase. *Proc Natl Acad Sci USA* **88**:2811–2814.

Hoque KE, Indorkar RP, Sammut S, and West AR (2010) Impact of dopamine-glutamate interactions on striatal neuronal nitric oxide synthase activity. *Psychopharmacology (Berl)* **207**:571–581.

Horner KA, Westwood SC, Hanson GR, and Keefe KA (2006) Multiple high doses of methamphetamine increase the number of preproneuropeptide Y mRNA-expressing neurons in the striatum of rat via a dopamine D1 receptor-dependent mechanism. *J Pharmacol Exp Ther* **319**:414–421.

Imam SZ, Crow JP, Newport GD, Islam F, Slikker W, Jr, and Ali SF (1999) Methamphetamine generates peroxynitrite and produces dopaminergic neurotoxicity in mice: protective effects of peroxynitrite decomposition catalyst. *Brain Res* **837**: 15–21.

Imam SZ, Islam F, Itzhak Y, Slikker W, Jr, and Ali SF (2000) Prevention of dopaminergic neurotoxicity by targeting nitric oxide and peroxynitrite: implications for the prevention of methamphetamine-induced neurotoxic damage. *Ann N Y Acad Sci* **914**:157–171.

Inoue H, Arai I, Shibata S, and Watanabe S (1996) NG-nitro-L-arginine methyl ester attenuates the maintenance and expression of methamphetamine-induced behavioral sensitization and enhancement of striatal dopamine release. *J Pharmacol Exp Ther* **277**:1424–1430.

Itzhak Y and Ali SF (1996) The neuronal nitric oxide synthase inhibitor, 7-nitroindazole, protects against methamphetamine-induced neurotoxicity in vivo. *J Neurochem* **67**:1770–1773.

Itzhak Y, Anderson KL, and Ali SF (2004) Differential response of nNOS knockout mice to MDMA ("ecstasy")- and methamphetamine-induced psychomotor sensitization and neurotoxicity. *Ann N Y Acad Sci* **1025**:119–128.

Itzhak Y, Gandia C, Huang PL, and Ali SF (1998) Resistance of neuronal nitric oxide synthase-deficient mice to methamphetamine-induced dopaminergic neurotoxicity. *J Pharmacol Exp Ther* **284**:1040–1047.

Itzhak Y, Martin JL, and Ail SF (2000a) nNOS inhibitors attenuate methamphetamine-induced dopaminergic neurotoxicity but not hyperthermia in mice. *Neuroreport* **11**:2943–2946.

Itzhak Y, Martin JL, and Ali SF (1999) Methamphetamine- and 1-methyl-4-phenyl-1,2,3, 6-tetrahydropyridine-induced dopaminergic neurotoxicity in inducible nitric oxide synthase-deficient mice. *Synapse* **34**:305–312.

Itzhak Y, Martin JL, and Ali SF (2000b) Comparison between the role of the neuronal and inducible nitric oxide synthase in methamphetamine-induced neurotoxicity and sensitization. *Ann N Y Acad Sci* **914**:104–111.

Iwahashi T, Inoue A, Koh CS, Shin TK, and Kim BS (1999) Expression and potential role of inducible nitric oxide synthase in the central nervous system of Theiler's murine encephalomyelitis virus-induced demyelinating disease. *Cell Immunol* **194**: 186–193.

Kawaguchi Y, Wilson CJ, Augood SJ, and Emson PC (1995) Striatal interneurones: chemical, physiological and morphological characterization. *Trends Neurosci* **18**: 527–535.

Keefe KA and Gerfen CR (1996) D1 dopamine receptor-mediated induction of zif268 and c-fos in the dopamine-depleted striatum: differential regulation and independence from NMDA receptors. *J Comp Neurol* **367**:165–176.

Kogan FJ, Nichols WK, and Gibb JW (1976) Influence of methamphetamine on nigral and striatal tyrosine hydroxylase activity and on striatal dopamine levels. *Eur J Pharmacol* **36**:363–371.

LaVoie MJ, Card JP, and Hastings TG (2004) Microglial activation precedes dopamine terminal pathology in methamphetamine-induced neurotoxicity. *Exp Neurol* **187**:47–57.

Le Moine C, Normand E, and Bloch B (1991) Phenotypical characterization of the rat striatal neurons expressing the D1 dopamine receptor gene. *Proc Natl Acad Sci USA* **88**:4205–4209.

Mark KA, Soghomonian JJ, and Yamamoto BK (2004) High-dose methamphetamine acutely activates the striatonigral pathway to increase striatal glutamate and mediate long-term dopamine toxicity. *J Neurosci* **24**:11449–11456.

Maxwell JC (2005) Emerging research on methamphetamine. *Curr Opin Psychiatry* **18**:235–242.

Morris BJ, Simpson CS, Mundell S, Maceachern K, Johnston HM, and Nolan AM (1997) Dynamic changes in NADPH-diaphorase staining reflect activity of nitric oxide synthase: evidence for a dopaminergic regulation of striatal nitric oxide release. *Neuropharmacology* **36**:1589–1599.

Nash JF and Yamamoto BK (1992) Methamphetamine neurotoxicity and striatal glutamate release: comparison to 3,4-methylenedioxymethamphetamine. *Brain Res* **581**:237–243.

O'Dell SJ, Weihmuller FB, and Marshall JF (1991) Multiple methamphetamine injections induce marked increases in extracellular striatal dopamine which correlate with subsequent neurotoxicity. *Brain Res* **564**:256–260.

O'Dell SJ, Weihmuller FB, and Marshall JF (1993) Methamphetamine-induced dopamine overflow and injury to striatal dopamine terminals: attenuation by dopamine D1 or D2 antagonists. *J Neurochem* **60**:1792–1799.

Oleszak EL, Katsetos CD, Kuzmak J, and Varadhachary A (1997) Inducible nitric oxide synthase in Theiler's murine encephalomyelitis virus infection. *J Virol* **71**: 3228–3235.

Park DJ and West AR (2009) Regulation of striatal nitric oxide synthesis by local dopamine and glutamate interactions. *J Neurochem* **111**:1457–1465.

Pastuzyn ED, Chapman DE, Wilcox KS, and Keefe KA (2012) Altered learning and Arc-regulated consolidation of learning in striatum by methamphetamine-induced neurotoxicity. *Neuropsychopharmacology* **37**:885–895.

Radi R, Beckman JS, Bush KM, and Freeman BA (1991) Peroxynitrite-induced membrane lipid peroxidation: the cytotoxic potential of superoxide and nitric oxide. *Arch Biochem Biophys* **288**:481–487.

Rushlow W, Flumerfelt BA, and Naus CC (1995) Colocalization of somatostatin, neuropeptide Y, and NADPH-diaphorase in the caudate-putamen of the rat. *J Comp Neurol* **351**:499–508.

Sammut S, Dec A, Mitchell D, Linardakis J, Ortiguela M, and West AR (2006) Phasic dopaminergic transmission increases NO efflux in the rat dorsal striatum via

a neuronal NOS and a dopamine D(1/5) receptor-dependent mechanism. *Neuropsychopharmacology* **31**:493–505.
Taraska T and Finnegan KT (1997) Nitric oxide and the neurotoxic effects of methamphetamine and 3,4-methylenedioxymethamphetamine. *J Pharmacol Exp Ther* **280**:941–947.
Thomas DM and Kuhn DM (2005) Attenuated microglial activation mediates tolerance to the neurotoxic effects of methamphetamine. *J Neurochem* **92**:790–797.
Uhl GR and Sasek CA (1986) Somatostatin mRNA: regional variation in hybridization densities in individual neurons. *J Neurosci* **6**:3258–3264.
Vaid RR, Yee BK, Rawlins JN, and Totterdell S (1996) NADPH-diaphorase reactive pyramidal neurons in Ammon's horn and the subiculum of the rat hippocampal formation. *Brain Res* **733**:31–40.
Volkow ND, Chang L, Wang GJ, Fowler JS, Leonido-Yee M, Franceschi D, Sedler MJ, Gatley SJ, Hitzemann R, and Ding YS, et al. (2001) Association of dopamine transporter reduction with psychomotor impairment in methamphetamine abusers. *Am J Psychiatry* **158**:377–382.
Wagner GC, Ricaurte GA, Seiden LS, Schuster CR, Miller RJ, and Westley J (1980) Long-lasting depletions of striatal dopamine and loss of dopamine uptake sites following repeated administration of methamphetamine. *Brain Res* **181**: 151–160.
Wang J and Angulo JA (2011) Synergism between methamphetamine and the neuropeptide substance P on the production of nitric oxide in the striatum of mice. *Brain Res* **1369**:131–139.
Wang J, Xu W, Ali SF, and Angulo JA (2008) Connection between the striatal neurokinin-1 receptor and nitric oxide formation during methamphetamine exposure. *Ann N Y Acad Sci* **1139**:164–171.
West AR and Galloway MP (1997) Endogenous nitric oxide facilitates striatal dopamine and glutamate efflux in vivo: role of ionotropic glutamate receptor-dependent mechanisms. *Neuropharmacology* **36**:1571–1581.
West AR, Galloway MP, and Grace AA (2002) Regulation of striatal dopamine neurotransmission by nitric oxide: effector pathways and signaling mechanisms. *Synapse* **44**:227–245.
Zhu J, Xu W, Wang J, Ali SF, and Angulo JA (2009) The neurokinin-1 receptor modulates the methamphetamine-induced striatal apoptosis and nitric oxide formation in mice. *J Neurochem* **111**:656–668.
Zhu JP, Xu W, and Angulo JA (2006) Distinct mechanisms mediating methamphetamine-induced neuronal apoptosis and dopamine terminal damage share the neuropeptide substance p in the striatum of mice. *Ann N Y Acad Sci* **1074**:135–148.
Zhu XZ and Luo LG (1992) Effect of nitroprusside (nitric oxide) on endogenous dopamine release from rat striatal slices. *J Neurochem* **59**:932–935.

Address correspondence to: Ashley N. Fricks-Gleason, Department of Pharmacology and Toxicology, 30 S 2000 East, Room 112, Salt Lake City, UT 84112. E-mail: a.fricks@utah.edu